Aspects of Nanotechnology

Research Article Open Access

Surface Density of Charged Functional Groups on Quantum Dots Determines Their Intracellular Compartmentalization and Biocompatibility

Yvonne Williams[1], Alyona Sukhanova[2], Jennifer Conroy[1,3], Bashir Mohamed[1], Vladimir Oleinikov[4], Mikhail Artemyev[4], Ciarán M Maguire[1], Igor Nabiev[1,2,4] and Yuri Volkov[1]**

[1]School of Medicine and AMBER Centre, Trinity College, the University of Dublin, Dublin 2, Ireland
[2]Laboratory of Research in Nanosciences, Université de Reims Champagne, France
[3]Nanolab Research Centre, FOCAS Institute, Dublin Institute of Technology, Dublin 8, Ireland
[4]Laboratory of Nano-Bioengineering, National Research Nuclear University MEPhI, Moscow, Russia

Abstract

Quantum Dots (QD) have a broad potential in the development of imaging, diagnostic and drug-delivery tools. Due to the homeostatic composition of biological systems, any charge on the surface of QD may influence penetration through the cell and organelle membranes, thus changing their cytotoxic effects.

The uptake, localization, and biocompatibility of CdSe/ZnS QD with varying ratios of Polyethylene glycol (PEG) derivatives to charged groups, were investigated in cultured cells using confocal microscopy and high content analysis. QD covered with amino-PEG derivative were predominantly localized in the perinuclear region and in the endoplasmic reticulum of both macrophage and epithelial cell lines, while QD functionalized with carboxy-PEG derivative remained in the cytosol. Furthermore, decreasing the density of cationic/carboxyl groups or increasing that of anionic/amino groups significantly improved cell viability. These findings may have considerable implications for using QD and other nanoparticles as imaging, diagnostic and drug-delivery tools in research and nanomedical applications.

Keywords

Nanoparticles, Quantum dots, Surface charge, Biocompatibility

Introduction

Evolution of eukaryotic cellular membranes has resulted in very efficient barriers while preserving specific permeability. Studies of these membranes have been limited due to inadequate tools for investigating events that occur at the nanoscale. The development of fluorescent nanocrystals or Quantum Dots (QD) has provided an exciting new research opportunity to probe these nanoevents [1].

Engineered nanoparticles are becoming increasingly a part of the fabric of modern life, in particular, nanomedicine, a new branch of medicine owing its very existence to nanomaterials. Their small size, positioning nanoparticles between atoms and many biological molecules, along with the possibility of varying surface functionality, makes them very suitable for use in conjunction with biomolecules [2]. Semiconductor QD are particularly promising as their fluorescent properties make them efficient multiparameter cellular probes: the QD emission wavelength can be simply altered by varying their size; and, unlike traditional fluorescent probes,

***Corresponding authors:** Yvonne Williams and Yuri Volkov, Trinity Centre for Health Sciences, James's Street, Dublin 8, Ireland, Tel: +353879863309, E-mail: williamy@tcd.ie; yvolkov@tcd.ie

Received: February 16, 2017: **Accepted:** July 25, 2017: **Published online:** July 27, 2017

Citation: Williams Y, Sukhanova A, Conroy J, et al. (2017) Surface Density of Charged Functional Groups on Quantum Dots Determines Their Intracellular Compartmentalization and Biocompatibility. Aspects Nanotechnol 1(1):20-31

they are more resistant to photobleaching, thus less likely to fade over the time frame of many experiments [3].

Controlled quantities of charged functional groups, usually amino (cationic), carboxyl (anionic), or hydroxyl (practically neutral) moieties [4], are required on the surface of QD to render them dispersible in aqueous media, enabling dispersion, and provide the valences necessary for their conjugation with biomolecules and enhancement of cellular uptake [5]. The use of multifunctional Polyethylene glycol (PEG) derivatives for nanoparticle solubilization or stabilization also provides the functionalities necessary to facilitate the biomolecule conjugation, and, *in vivo*, prevents particle uptake by the reticulo-endothelial system [6].

The distribution of particles in the body is largely governed, not only by their size [7], but also by their charge [8]. Those with carboxyl groups target the lungs and liver and are also more likely to remain in circulation [9]. Neutral and anionic nanoparticles have been shown to carry colloidal drugs across the blood-brain barrier without any adverse effects, while cationic particles may have a more immediate toxic effect [10]. However, since the toxicity of cationic particles is believed to be due to activation of the inflammatory response, it could be possible to harness this outcome to control autoimmune diseases [11].

The phospholipid bilayer of the cell membrane can have different charges, depending on the surrounding pH. If the pH is neutral, most phospholipids will have a negative or neutral charge, with only a few having a positive charge [12]. Initially, it was believed that positively charged QD are more likely to be taken up by cells [13], and it seemed counter-intuitive that negatively charged particles could enter the cell and migrate towards a nucleus packed with negatively charged nucleic acids. However, studies have shown that negatively charged QD not only enter the nucleus [14], but also have tropism for positively charged histones [15]. More recently, many authors have reported that negatively charged QD enter the cells and appear to be better tolerated than positively charged QD [16,17]. Internalization of nanoparticles is not fully understood and is believed to be multifactorial, depending on the nanoparticle size, charge, and shape [18,19]. Surface cationic nanoparticles are taken up by phagocytosis, which indicates that these particles form aggregates, because particles should be approximately 2 μm in size for optimal phagocytosis [20], although a recent study has shown that caveolae and dynamin-dependent mechanisms may be involved in the uptake of cationic gold nanoparticles [21]. Neutral QD with hydroxyl groups on the surface are less interactive with cell membranes and, hence, less toxic [22]. The lower pH inside endosomes may alter the resultant charge of the cell interior, thereby determining whether the particles end up in the acidic lysosomes or in the endoplasmic reticulum [23]. Furthermore, the presence of amine groups on QD within the endosomes may result in the "proton sponge" effect leading to chlorine accumulation, endosome swelling and rupture, and release of the QD into the cytosol, thus preventing the possible destruction of QD in the lysosomes [24].

There is much evidence that cadmium-containing QD are cytotoxic [25]. Studies on QD cytotoxicity have shown that particle size [13], charge [26], leakage of cadmium from the QD core [27], as well as ligands and surface chemistry [28,29] may also be factors of QD toxicity. Furthermore, there are conflicting reports as to whether cationic [26,30], or anionic [9,31] functional groups are the more toxic. However, as an electric charge alters hydrophilicity, this may reduce any cytotoxic effect [3]. Particles with hydroxyl groups, which have a neutral charge, have generally been considered to have a very low toxicity [22], but this may be due to the QD not being internalized as rapidly as cationic or anionic particles [32]. Some studies have even suggested that it is more the surface functionalities than the actual QD itself that result in cytotoxicity [33,34].

Previously CdSe/ZnS QD (3.1 nm, λ_{em} = 570 nm) have been demonstrated to be localized mainly in the nucleus of macrophages while alternatively in epithelial cells, QD remained in the cytosol [7]. For the purpose of this study, these same QD were further functionalized with different ratios of monodispersed derivatives of PEG, all containing free thiol and different terminal amine ($-NH_2$), carboxyl (-COOH), or hydroxyl (-OH) groups [35] and introduced into cultured human cells.

Confocal microscopy and automated microscopic High Content Imaging and Analysis Platforms (HCA) were used to obtain and both qualitatively and quantitatively analyze images for biolocalisation and cytotoxicity of QD as previously described [7,36].

Presented here are the results of a systematic investigation of intracellular internalization of anionic and cationic QDs. Experiments are shown that variations of the ratio between amino and hydroxyl groups or, alternatively, carboxyl and hydroxyl groups on the QD surface could give valuable insight into the patterns of charge distribution within cells of various lineages. Furthermore, this made it possible to optimize the QD localization while decreasing toxicity.

Material and Methods

Quantum dots

Synthesis and solubilization of nanocrystals: Core/shell CdSe/ZnS QD, with a fluorescent core of cadmium selenide and a zinc sulfide shell were synthesized and

solubilized in water using the previously published procedures [35]. Briefly, QD were first transferred into water after attachment of DL-Cysteine (DL-Cys) (Sigma, St Louis, USA) to their surface, as described earlier [37,38]. The resulting water-dispersible QD displayed a bright photoluminescence (PL) with a quantum yield close to 60% at room temperature.

Then, DL-Cys on the QD surface was replaced with a thiol-containing monodispersed PEG derivative with a terminal hydroxyl group (HS-C11-EG6) or a mixture of thiol-containing PEG derivatives with terminal carboxyl (HS-C11-EG6-OCH_2-COOH) and hydroxyl groups or terminal amino (HS-C11-EG6-NH_2) and hydroxyl groups (ProChimia Surfaces, Sopot, Poland). C11 undecyl chain terminated with thiol used for increase the stability of PEG-shell of QD and EG6 PEG repeat units was sufficient to obtain the samples of QD perfectly dispersible in water and biological buffers. The mixtures of the polymers used for QD solubilization were adjusted to provide the lowest possible nonspecific binding of QD to cells and tissues. QD surface treatment with low-molecular-weight PEG-based polymers yields water-dispersible CdSe/ZnS QD with the smallest possible diameter [35]. The optimal results were obtained with shells consisting of HS-C11-EG6 alone or 95% of HS-C11-EG6 and 5% of HS-C11-EG6-NH_2.

Briefly, 156 µl of a 150 mg/ml aqueous solution of HS-C11-EG6 or a mixture of 15 µl of 100 mg/ml of HS-C11-EG6-NH_2 and 150 µl of 150 mg/ml of HS-C11-EG6 were added to 1 ml of preparations of QD-Cys in pure water (10 mg/ml). The samples were incubated overnight at 4 °C, pre-cleaned by centrifugation using Amicon Ultra-15 filter units with a 10 kDa cut-off (Millipore) and finally purified from excess of ligands by gel exclusion chromatography on Sephadex G-25 (Sigma) columns.

To obtain differentially charged QD, the mixtures with different percentages of HS-C11-EG6-NH_2 and HS-C11-EG6 derivatives or HS-C11-EG6-OCH_2-COOH and HS-C11-EG6 derivatives were used for modification of the surface of QD-Cys. The samples were incubated overnight at 4 °C, pre-cleaned by centrifugation using Amicon Ultra-15 filter units with a 10 kDa cut-off (Millipore), and finally purified from excess of ligands by gel exclusion chromatography on Sephadex G-25 (Sigma) columns. The functional QD surface charge is expressed as percentages of differently charged derivatives of PEGs used for functionalization of the QD surface, i.e., CdSe/ZnS n% (amine or carboxyl) (100-n)% OH. For clarity, the following abbreviations are used: 5% NH_2QD, 20% NH_2QD, 40% NH_2QD, 100% NH_2QD, 10% COOH QD, 40% COOH QD, 60% COOH QD, 100% COOH QD, and (for the neutral hydroxyl PEG derivative) 100% OH QD. It should be noted that the quantum yield of QD does not change upon ligand exchanges at the surface and it was the same for all QD samples.

Quantum dot characterization: The diameters and extinction coefficients of CdSe/ZnS QD were calculated as described by Yu, et al. [39], and corrected according to more recent data [40]:

$$D = (1.6122\times10^{-9})\lambda^4 - (2.6575\times10^{-6})\lambda^3 + (1.6242\times10^{-3})\lambda^2 - (0.4277)\lambda + 41.57$$

and $\epsilon = 1600\Delta E(D)^3$

Where D is the size of the nanocrystal (nm), λ is the wavelength of the first excitonic absorption peak (nm), ε is the extinction coefficient per mole of nanocrystal and ΔE is the transition energy corresponding to the first absorption peak in electron volts (eV).

The characteristics of the QD prepared were estimated using Dynamic Light Scattering (DLS) by means of a Zetasizer Nano ZS device (Malvern Instruments, Worcestershire, UK). Samples in cell culture media (RPMI 1640) supplemented with Fetal Calf Serum (FCS) and glutamine) were filtered through a 0.1 µm filter, and particle size distribution was measured at 25°C in a low-volume quartz batch cuvette (Hellma ZEN2112). The hydrodynamic sizes were calculated from diffusion times using the Stokes-Einstein equation. The results were obtained by measuring the scattering intensity (10 runs per measurement) for each sample. All measurements were performed in triplicate, and the average values were used to calculate the hydrodynamic diameters according to the CONTIN algorithm.

Absorbance spectra were recorded using a Cary 50 Conc. UV-V is spectrophotometer (Varian, USA). Photoluminescence measurements were carried out using a Cary Eclipse spectrofluorimeter (Varian, USA) (λ_{ex} = 400 nm).

Cell culture

Two different types of cell lines were used to investigate the internalization of the QDs: the HEp-2 human epithelial HeLa cell derivative carcinoma cell line (ECACC, UK) grown in minimum essential medium (Eagle) with Earles Salts (Sigma Aldrich UK) and the THP-1 human acute monocytic leukemia monocyte line (ECACC, UK) grown in RPMI 1640 medium (Sigma Aldrich UK). Epithelial cells and macrophages are the first line of defense for the immune system and therefore suitable cells to use in the investigation of biocompatibility and intracellular localization of nanoparticles [2]. It was expected that both cell lines would exhibit different uptake and transport mechanisms based on the functionality of the original cell line [20,23].

Both cell culture media were supplemented with

10% Foetal Calf serum (FCS) (Sigma Aldrich UK), 200 mM L-glutamine, 10,000 U/ml penicillin, and 10 mg/ml streptomycin. After 5 passages post reconstitution the cells were plated into 96 well microtitre plates and onto coverslips at a concentration of 2×10^5 cells/ml. The THP-1 cells were incubated in the presence of 100 ng/ml phorbal 12-myristate-13-acetate, a mitogen, to enable monocyte to macrophage differentiation. Cell lines were maintained under controlled atmospheric conditions of 37 °C and 5% CO_2. HEp-2 cells were cultured for 24 hours until reaching an 80% confluence, with macrophage differentiation taking place over 72 hours for the THP-1 cell line. The cells were then exposed to modified QD and unmodified QD under physiological conditions. Also cells grown in the exact same conditions, but in the absence of QD were used as a baseline control. All QD solutions were diluted with culture medium to a final concentration of 0.2 mg/ml. Then 50% of the media (100 µl/well from the 96 well plate; 200 µl/well from the 8-well plate) was replaced with the diluted QD, and the cells were cultured for another 3 hours. The cells were then counterstained with 1 mg/ml Hoechst 33342 (Molecular Probes, USA) for 3 minutes and fixed with 2% paraformaldehyde as previously described [41].

Preparation of permeabilized fixed cells: Both HEp2 and THP-1 cells were fixed and then permeabilized in order to eliminate the differences conferred by lineage-specific transport mechanisms, including the effect of pH on the QD charge [41,42]. A stock solution of 6% Paraformaldehyde (PFA) in Phosphate Buffer Saline (PBS) was made and stored at room temperature. A 0.5% solution of Triton™ X-100 (Sigma-Aldrich, UK) in PBS was used to permeabilize the PFA-fixed cells. The cells were left in PBS at 4 °C, until required. PBS was replaced with 100 µl of media, and 100 µl of the diluted QD solution was added. The cells were incubated in the presence of the QD for 1 hour at room temperature, washed with fresh medium, counterstained with Hoechst as before, finally washed, and prepared for microscopic analysis.

Viability studies

The cell number, and the size of their nuclei, as determined using a KineticScan® HCS reader (Thermo Fisher, CA, USA) and Compartmental Analysis BioApplication software (Thermo Fisher, CA, USA) were compared with those of control cells to estimate the proportion of viable cells [43]. An increase in the nucleus size suggests an arrested cell cycle, whereas a decreased size and an increased fluorescent intensity are indicative of nuclear condensation and programmed cell death. The significance of results was calculated using One-way Analysis of Variance (ANOVA) on GraphPad InStat® for Macs Version 3.1 (2009) software.

A time course study was performed, adding 5% NH_2QD to macrophages at intervals of 15, 30, 60, 90, and 120 minutes. The results were then analyzed by means of HCA.

Additionally, macrophages were incubated with 5% NH_2QD under standard culture conditions for four weeks. The medium was changed every two days by replacing 50% of the culture medium with fresh medium. Daily observation was carried out using confocal microscopy.

Fluorescence microscopy

Images of cells in the microtitre plates were obtained using the KineticScan® HCS reader (Thermo Fisher, CA, USA) and subsequently analyzed by means of Toolbox Scan® with the Compartmental Analysis BioApplication® software (Thermo Fisher, CA, USA). The cell nuclei were identified by Hoechst staining using a bandpass filter with λ_{Ex} = 360(50) and λ_{Em} = 515(20); QD emitting at 570 nm (QD570) and 600 nm (QD600) were detected using bandpass filters with λ_{Ex} = 475(40), λ_{Em} = 515(20) and λ_{Ex} = 560(15), λ_{Em} = 600(25), respectively. Manual investigation of the QD entry and distribution in the live cells was carried out by means of a Nikon Eclipse TE 300 fluorescence microscope and an UltraView Live Cell Imager confocal microscopy workstation (PerkinElmer Life Sciences, Warrington, UK).

Results

Properties of quantum dots

CdSe/ZnS QDs were synthesized as previously reported [35] and PEGylated to facilitate the attachment of functional groups. The absorption and PL spectra of the synthesized and solubilized CdSe/ZnS QD are shown in Figure S1 [44]. The results of QD characterization including hydrodynamic and "physical" diameters and zeta-potentials are shown in Table 1 and Table 2. The percentage of amino groups ranged from 5% to 100%, and that of carboxyl groups ranged from 10% to 100%. The QD core had a diameter of approximately 3.1 nm (λ_{em} = 570); 100% COOH QD with core diameters of approximately 4.6 nm (λ_{em} = 600) were also included to demonstrate the influence of charge with respect to size. 100% OH QD were included for completeness but as reported in other studies [31] had no adverse effect on cell viability and generally localized on or near the cell membrane.

Quantitative data on QD biocompatibility, i.e. changes in the cell number and nuclear size, are shown as bar charts in Figure 1, while portrayal of the resultant QD intracellular compartmentalization is summarized in Figure 2. Also included in Figure 2 are schematic mechanisms of nanoparticle uptake summarizing previous

Table 1: Properties of quantum dots after their solubilization with DL-Cys.

Sample*	PL emission peak (nm)	Quantum yield (%)	Diameter (nm)**	Hydrodynamic diameter (nm)***	ζ-potential (mV)
QD570					
CdSe/ZnS-Cys	570	48	3.1	6 ± 2	-33.4
QD600					
CdSe/ZnS-Cys	599	42	4.6	7 ± 2	-37.5

*For all measurements, QD concentrations of about 0.5-1.5 μM were used. In all cases, the absorbance at the first excitation band was < 0.10; **Diameters of the fluorescing CdSe cores of CdSe/ZnS QDs were calculated as previously described [38], then corrected, where necessary, according to Jasieniak, *et al.* [40]; ***The hydrodynamic diameters were measured using the Dynamic Light Scattering (DLS) technique as previously described [44]. The mean values and standard deviations for three independent experiments are shown.

Table 2: Physicochemical properties and relative capacities of nonspecific binding to the cell membrane for CdSe/ZnS QD570 encapsulated with mixtures of PEG-based polymers with different charges.

QD surface functionalities	PL emission peak (nm)	ζ potential (mV)	Relative nonspecific binding of QDs to cell membrane
100%PEG-OH	568	-6	10%
95%PEG-OH + 5% PEG-NH_2	568	6	20%
80%PEG-OH + 20% PEG-NH_2	570	17.5	40%
60%PEG-OH + 40% PEG-NH_2	571	36.7	60%
100% PEG-NH_2	573	43	100%
100%PEG-COOH	566	-36	100%
60%PEG-COOH + 40%PEG-OH	567	-28.1	60%
40%PEG-COOH + 60%PEG-OH	568	-20.4	35%
10%PEG-COOH + 90%PEG-OH	569	-15	30%

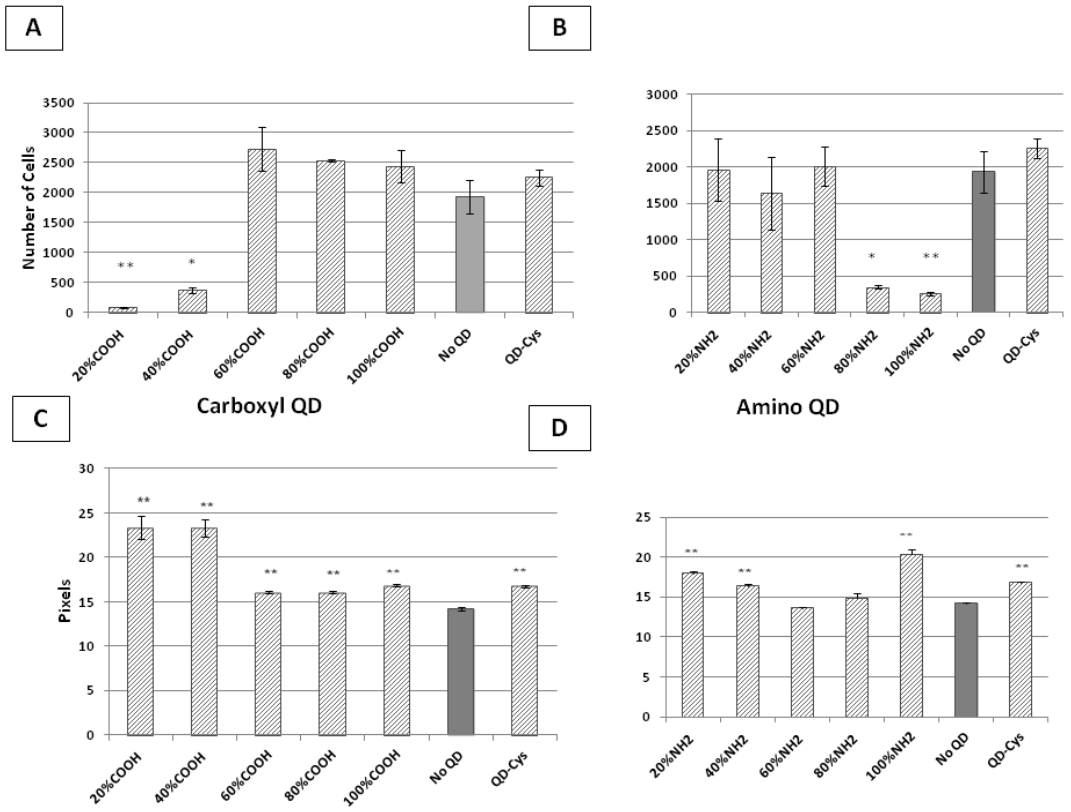

Figure 1: Biocompatibility of charged QD with epithelial cells.

The number of cells over three separate experiments (A,B) and the mean nuclear size (in pixels) (C,D) with the standard error of the mean in epithelial cells exposed to carboxyl (A,C), and amino (B,D) QD. The exposure to unmodified QD (QD-Cys) is also shown. The shaded columns represent cells not exposed to QD.

*$p < 0.05$, **$p < 0.01$ One-way Analysis Of Variance (ANOVA).

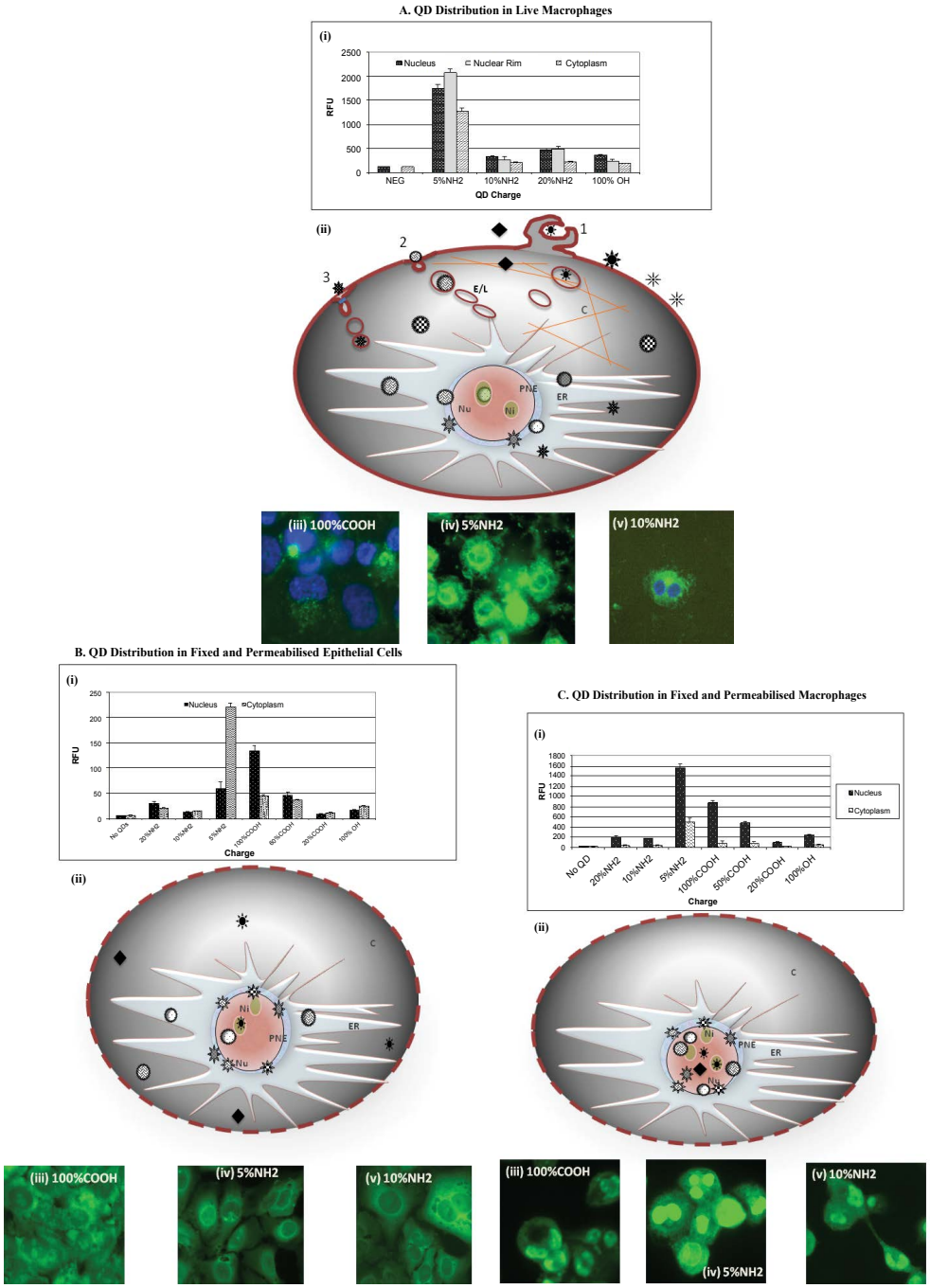

Figure 2: Distribution of charged QD in (A) Live macrophage cells; (B) Fixed and permeabilized epithelial cells, and (C) Fixed and permeabilized macrophages.

(i) Graph showing quantitative distribution of cytoplasmic and nuclear fluorescence ie QD localization, within the cells; RFU: Relative Fluorescent Units; (ii) Schematic representation of localization of anionic and cationic QD within the cytoplasm and nucleus of the cell.

Three endocytic mechanisms are depicted: (1) Phagocytosis; (2) Macrocytosis and (3) Clathrin-Mediated Endocytosis.

C: Cytoplasm; E/L: Endosomes/Lysosomes; ER: Endoplasmic Reticulum; Nu: Nucleus; Ni: Nucleoli; PNE: Perinuclear Envelope.

Amino-, carboxyl-, and hydroxyl-functionalized QD are shown as circle, star, and diamond symbols, respectively. The charge density (the proportion of amino/carboxyl/hydroxyl groups) decreases with decreasing shading:

○ 5% NH_2QD; ◍ 20% NH_2QD; ◉ 40% NH_2QD; ● 60% NH_2;

✸ 20% COOH QD; ✵ 40% COOH QD; ✸ 60% COOH QD; ✸ 100% COOH QD (570 nm); ✳ 100% COOH QD (600 nm);

♦ 100% OH QD.

Confocal images of cultured cells are shown stained with green fluorescence indicating localization of (iii) 100% COOH QD; (iv) 5% NH_2QD and (v) 10% NH_2QD.

published and well-established data [45-47].

Intracellular compartmentalization of anionic quantum dots

The toxicity of carboxylated (anionic) QD decreased when the percentage of HS-C11-EG6-OCH_2-COOH, used for QD solubilization, was increased. The 20% COOH and 40% COOH QD elicit a strong cytotoxic response in both living epithelial and macrophage cells, resulting in a radical decrease in cell number ($p < 0.01$) (Figure 1A), thus making specific localization difficult to establish. Furthermore, the increase ($p < 0.01$) in the nuclear size in these cells suggests an arrested cell cycle, although the small number of cells (Figure 1C) prevents any definitive conclusion. The increase in cell number in the presence of the 60 and 80% COOH QD is not fully understood, but may be that these cells were stimulated by the presence of QD in the cytoplasm. However there may also be an artifact of the assay, as there was no significant difference ($p > 0.05$) between the cell numbers of these QD and of cells not exposed to QD or those exposed to QD without the functional groups attached (ie cysteine coated QD).

The proportion of carboxyl groups present on the surface of the QDs, and ultimately their surface charge, resulted in various uptake patterns within the cells. QDs with low proportions of carboxyl groups were internalized further within the cells. 100% COOH QD were observed to accumulate at the cell surface, with 80% COOH QD forming a "reticular" fluorescent pattern in the cytoplasm and 60% COOH QD forming a punctuate pattern at the nuclear membrane. Of note the effect of QD size was less crucial as both 3.1 nm (λ_{em} = 570 nm) and 4.6 nm (λ_{em} = 600 nm) 100% COOH QD remained at the epithelial cell surface (Figure S2A and Figure S2B), although in the macrophages these same QD accumulated in lysosomes, apparently reflecting the phagocytic process as a functional specialization of macrophages (Figure 2A, iii).

Intracellular compartmentalization of cationic quantum dots

In contrast to the anionic QD, cells exposed to amino (cationic) QD (covered with HS-C11-EG6-NH_2) were observed to have decreasing viability as the proportion of NH_2 groups increased (Figure 1B). The 80% NH_2 and 60% NH_2QD aggregated, precipitating out of suspension, thus not entering cells. In addition, the nuclei of the cells exposed to these particles were smaller ($p < 0.01$) than the control cells (Figure 1D), supporting published data on the toxicity of cationic QD [18,26].

Comparison of epithelial cell biocompatibility with 100% COOH QD (Figure S2A) and 100% NH_2QD (Figure S2C) demonstrates the relatively low level of toxicity of carboxyl-coated QD.

When internalized into cells, if there was a low density of amino groups on their surface, the cationic QD compartmentalized closer to nucleus than the anionic QD. The 60% NH_2 and 40% NH_2QD were internalized into the cytoplasm of epithelial cells, with some evidence of toxicity, while 5% NH_2QD accumulated at the nuclear membrane of healthy cells (Figure 2A, iv). In macrophages, NH_2QD with low surface charge density (20%) appeared as a diffuse meshwork pattern of fluorescence concentrating towards the perinuclear space, which suggested QD localization within the Endoplasmic Reticulum (ER) (Figure 2A, v).

Thus, we observed a decreased viability in the cells exposed to QD with either a high percentage of amino groups or a low percentage of carboxyl groups on their surface. This suggests that the QD can be rendered less toxic by decreasing the cationic charge or increasing the anionic charge. Furthermore, positively charged QD more easily penetrate into the perinuclear area. Consequently, weakly cationic QD could be advantageous in applications involving living cells.

Properties of weakly cationic quantum dots

Although 5% NH_2QD were synthesized by the same method as the other QD studied, their localization in cellular compartments was characteristic of both the amino- and carboxyl-coated particles. They appeared to be taken up by the ER system and transported to the perinuclear area, to be eventually located within the nucleoli. Figure 3 demonstrates the time course of the accumulation of 5% NH_2QD in macrophages. Initially, after 15 min of incubation, the QD could be seen as a delicate linear staining highlighting the cell periphery corresponding to the plasma membrane (Figure 3A). Later, they moved into the cytoplasm, with homogeneous staining observed after 30 min of incubation (Figure 3B) and a more reticular pattern, by the 60th minute of incubation (Figure 3C). After 90 min, the reticular staining was more pronounced; the QD were accumulating in the perinuclear area and disappeared from the cell perimeter (Figure 3D). Eventually, after 150 min of incubation, the QD-associated fluorescence was mainly concentrated to the nuclear envelope and the nucleoli (Figure 3E). The increase in the fluorescent intensity caused by the entry of QD into the four main cellular compartments is shown in Figure 3F. The process of nanoparticle uptake is continuous and is considered a commonly irreversible occurrence with no clear process of exocytosis as yet confirmed. This appears then as an overall fluorescence increase above all compartments over time.

Experiments on continuous exposure of differenti-

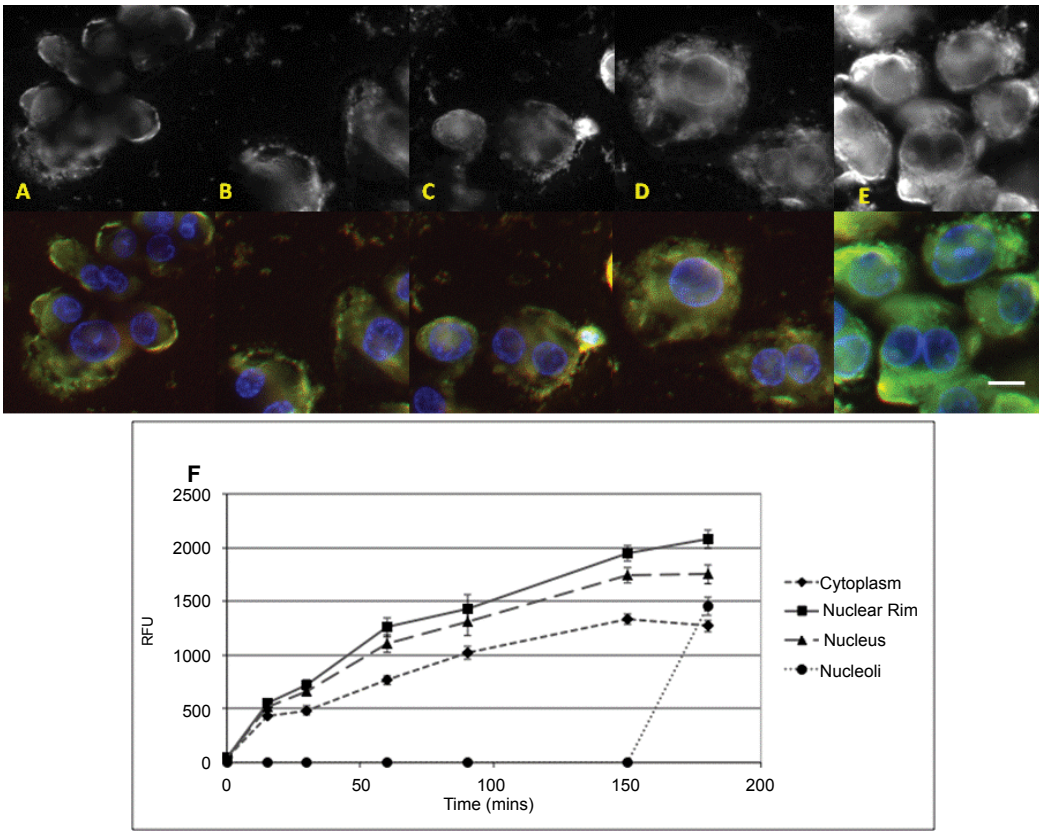

Figure 3: Time course of 5% NH_2QD localization in macrophages.

Top row: greyscale fluorescent image of QD distribution in macrophages after (A) 15; (B) 30; (C) 60; (D) 90 and (E) 150 minutes.

Bottom row: color overlay of nuclear staining (blue fluorescence) and 5% NH_2QD emission (green fluorescence). Scale bar is 10 µm.

(F) Relative fluorescence intensity of 5% NH_2QD over time in the cytoplasm, perinuclear area, nucleus, and nucleoli. Images were obtained and analyzed using a KineticScan® device (Thermo Fisher, CA, USA). The results represent the mean intensity and the standard error of the mean. RFU: Relative Fluorescent Units.

ated (non-proliferating) macrophages to 5% NH_2QD for more than 4 weeks demonstrated long-term biocompatibility of these QD. Although the nanoparticles did precipitate out of solution over the long period of time, the macrophages appeared to retain the ingested QD without any apparent adverse effects on the cells. Furthermore, phagokinetic tracks were observed around the adherent cells against the brightly fluorescent background of precipitated QD, indicating continuous cellular uptake (Figure 4).

Charged quantum dots in fixed permeabilized macrophages and epithelial cells

Charged QD were observed in cultured cells fixed after permeabilization of the cell membrane as described above (Figure 2B). In contrast to the experiments on living cells, 100% and (to a lesser extent) 50% carboxyl QD were located in the nucleoli of epithelial cells, being probably associated with positively charged histones [15]. All the other COOH QD appears to concentrate in the perinuclear recycling compartment, also observed by Barua and Rege [48] (Figure 2B, ii and Figure 2B, iv). Furthermore, the cationic QD had a more cytosolic distribution and may be localized within the ER (Figure 2B, ii and Figure 2B, iii). Conversely, while this reversed localization was observed in fixed permeabilized epithelial cells, localization of QD in fixed permeabilized macrophages were mainly determined by the QD size (~3.1 nm; λ_{em} = 570 nm), [13,14] and were found in the nucleus irrespective of their charge (Figure 2C).

Discussion

Significant concern regarding the toxicity of semiconductor QD limits their potential nanomedical applications. However, there is a strong possibility that these fascinating particles could serve as powerful tools in *ex vivo* analysis of living cells. While QD internalization into the cell has not been fully elucidated, it is believed to occur by macropinocytosis [49] and/or clatherin-independent endocytosis [14]. This study clearly demonstrates that controlled variation of the QD surface charge by using different proportions of HS-C11-EG6-NH_2 and HS-C11-EG6 moieties or HS-C11-EG6-OCH_2-COOH and

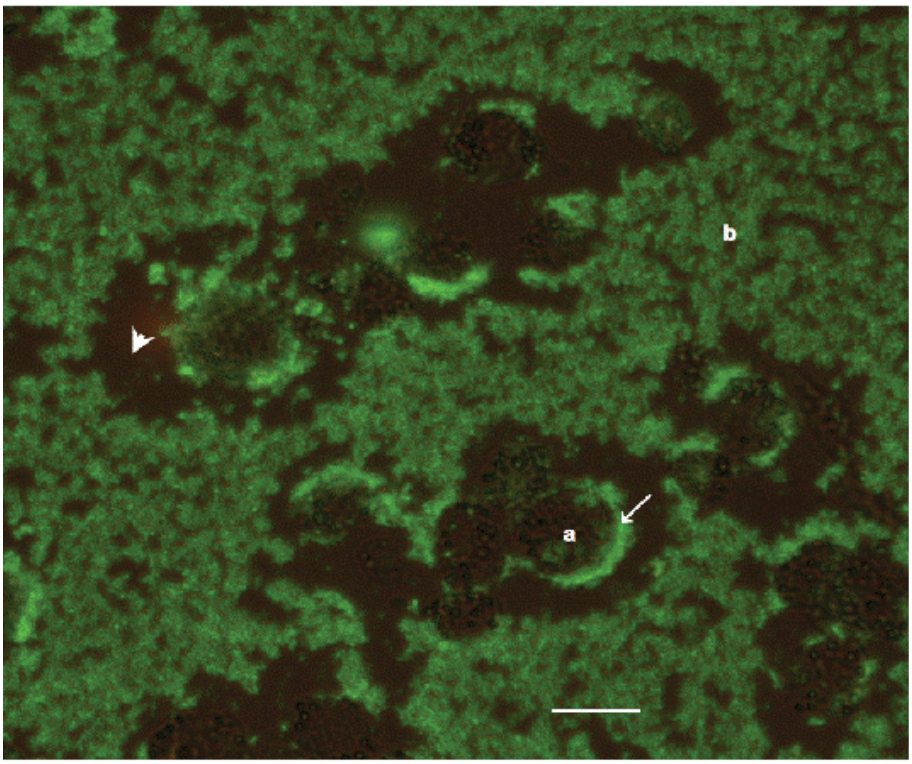

Figure 4: Macrophages in culture in the presence of 5% NH_2QD.

Simultaneous fluorescent and transmitted background light image of macrophages (A) among precipitated 5% NH_2QD; (B) with the fluorescent QD accumulating at the cell membrane **(↖)** before being internalized by the cell, leaving behind phagokinetic tracks **(➤)**. Scale bar is 10 μm.

HS-C11-EG6 moieties for QD functionalization influences the specifics of nanoparticle localization in the cell, and this appears to be related to the relative densities of COOH, OH, and NH_2 groups on the QD surface. This has strong implications for the use of QD and, probably, other nanoparticles of similar sizes as probes in the study of cellular homeostasis and their applications as diagnostic probes and drug delivery tools in the *ex-vivo* setting [45].

Furthermore, decreasing the proportion of amino groups or increasing that of carboxyl groups appears to render QD less toxic to the cell lines tested in this study. While the amount of charged functional groups on the particles is not linearly related to the actual charge (or zeta potential) of QD, the nature of the surface functionalities (amino, hydroxyl, or carboxyl groups) determines the specific QD distribution pattern and, as a result, their biocompatibility. Moreover, advanced approaches to surface passivation of QD might open up new avenues in the development of biocompatible QD-based research and diagnostic tools [35].

The particle surface charge has a dynamic and kinetic influence on the interaction of the particle with the cell; therefore, it was crucial for the purposes of this study that live cells be examined in terms of QD localization patterns in different cell types and any possible effect of QD on cell viability. However, if cells were fixed and permeabilized prior to the addition of QD, any effects related to active QD uptake mechanisms or specificity of signaling routes in different cell types were eliminated, and a snapshot of cellular homeostasis at a particular moment of time could be obtained. This would suggest that electrostatic variability within the cell or within individual cytoplasmic compartments is partly attenuated by the process of fixation [50]. In addition, epithelial cells are characterized by basal-apical polarity, thus requiring a more ordered organization of the cellular matrix [51], which makes them less prone to damage by the permeabilization and fixation procedures.

These findings clearly indicate that surface passivation (PEGylation) of otherwise highly toxic particles could render them considerably more biocompatible, at least in our models which are representative of phagocytic and epithelial cells. Recently, Nagy, et al. showed similar findings in primary human lung cells [33], however, further studies with other models would need to be performed to extrapolate to other biosystems. Our study is the first to demonstrate the possibility of prolonged biopersistance of surface-passivated QD in living human cells.

The observed effects at the cellular level are generally reproducible with any particular batch of QD, and implementing HCA platforms enables accumulation of large amounts of robust and consistent data. However,

an ongoing issue with the studies of nanoparticles in biomedical settings is the imperfection of methods for synthesizing particles with reproducible characteristics and the resultant batch-to-batch variability, especially in the case of nanomaterials used in aqueous media [32]. Therefore, further development of QD with advanced properties may be fraught with difficulties in trying to standardize the manufacturing conditions for obtaining QD with identical characteristics.

In conclusion, charged functional groups on the nanoparticle surface may affect their intracellular compartmentalization, biocompatibility, and toxicity, thereby demonstrating application opportunities for finely tuned charged nanoparticles in the treatment of diseases requiring precisely targeted intracellular drug delivery and/or cell destruction, such as malignancies and certain types of autoimmune processes [45].

Acknowledgements

This study was supported, in parts, by the European Commission through the FP7 Cooperation Program (project NAMDIATREAM, Grant #NMP4-LA-2010-246479), by the Higher Education Authority of Ireland, Science Foundation of Ireland through the Advanced Materials and BioEngineering Research (AMBER) project (Grant #SFI/12/RC/2278) and by the Agence Nationale de Recherche (France) through the ICENAP project of the M-ERA. NET EU Programme (contract no. ANR-14-MERA-0002), and by the Russian Science Foundation (contract no. 17-15-01533).

We thank Dr. Anthony Davies for the help with High Content Screening and Analysis studies.

References

1. Xia T, Rome L, Nel A (2008) Nanobiology: Particles slip cell security. Nat Mater 7: 519-520.
2. McNeil SE (2005) Nanotechnology for the biologist. J Leukoc Biol 78: 585-594.
3. Alivisatos AP, Gu W, Larabell C (2005) Quantum dots as cellular probes. Annu Rev Biomed Eng 7: 55-76.
4. Hoshino A, Fujioka K, Oku T, et al. (2004) Physicochemical properties and cellular toxicity of nanocrystal Quantum Dots depend on their surface modification. Nano Lett 4: 2163-2169.
5. Parak WJ, Pellegrino T, Plank C (2005) Labelling of cells with quantum dots. Nanotechnology 16: 9-25.
6. Bentzen EL, Tomlinson ID, Mason J, et al. (2005) Surface modification to reduce nonspecific binding of quantum dots in live cell assays. Bioconjug Chem 16: 1488-1494.
7. Williams Y, Sukhanova A, Nowostawska M, et al. (2009) Probing cell-type-specific intracellular nanoscale barriers using size-tuned quantum dots. Small 5: 2581-2588.
8. Minchin R (2008) Nanomedicine: Sizing up targets with nanoparticles. Nat Nano 3: 12-13.
9. Quentin le Masne de Chermont, Corinne Chanéac, Johanne Seguin, et al. (2007) Nanoprobes with near-infrared persistent luminescence for in vivo imaging. Proc Natl Acad Sci USA 104: 9266-9271.
10. Lockman PR, Koziara JM, Mumper RJ, et al. (2004) Nanoparticle surface charges alter blood-brain barrier integrity and permeability. J Drug Target 12: 635-641.
11. Dong L, Xia S, Chen H, et al. (2010) Anti-arthritis activity of cationic materials. J Cell Mol Med 14: 2015-2024.
12. Lodish H, Baltimore D, Berk A (1995) Molecular Cell Biology. (3rd edn), WH Freeman & Co.
13. Lovric J, Bazzi HS, Cuie Y, et al. (2005) Differences in subcellular distribution and toxicity of green and red emitting CdTe quantum dots. J Mol Med (Berl) 83: 377-385.
14. Nabiev I, Mitchell S, Davies A, et al. (2007) Nonfunctionalized nanocrystals can exploit a cell's active transport machinery delivering them to specific nuclear and cytoplasmic compartments. Nano Lett 7: 3452-3461.
15. Conroy J, Byrne SJ, Gun'ko YK, et al. (2008) CdTe nanoparticles display tropism to core histones and histone-rich cell organelles. Small 4: 2006-2015.
16. dos Santos T, Varela J, Lynch I, et al. (2011) Quantitative assessment of the comparative nanoparticle-uptake efficiency of a range of cell lines. Small 7: 3341-3349.
17. Choi HS, Ashitate Y, Lee JH, et al. (2010) Rapid translocation of nanoparticles from the lung airspaces to the body. Nat Biotechnol 28: 1300-1303.
18. Verma A, Stellacci F (2010) Effect of surface properties on nanoparticle-cell interactions. Small 6: 12-21.
19. Xu A, Yao M, Xu G, et al. (2012) A physical model for the size-dependent cellular uptake of nanoparticles modified with cationic surfactants. Int J Nanomed 7: 3547-3554.
20. Champion JA, Walker A, Mitragotri S (2008) Role of particle size in phagocytosis of polymeric microspheres. Pharm Res 25: 1815-1821.
21. Saha K, Kim ST, Yan B, et al. (2012) Surface functionality of nanoparticles determines cellular uptake mechanisms in mammalian cells. Small 9: 300-305.
22. Kairdolf BA, Mancini MC, Smith AM, et al. (2008) Minimizing nonspecific cellular binding of quantum dots with hydroxyl-derivatized surface coatings. Anal Chem 80: 3029-3034.
23. Maxfield FR, McGraw TE (2004) Endocytic recycling. Nat Rev Mol Cell Biol 5: 121-132.
24. Yezhelyev MV, Qi L, O'Regan RM, et al. (2008) Proton-sponge coated quantum dots for siRNA delivery and intracellular imaging. J Am Chem Soc 130: 9006-9012.
25. Lewinski N, Colvin V, Drezek R (2008) Cytotoxicity of nanoparticles. Small 4: 26-49.
26. Leroueil PR, Berry SA, Duthie K, et al. (2008) Wide varieties of cationic nanoparticles induce defects in supported lipid bilayers. Nano Lett 8: 420-424.
27. Tarantola M, Schneider D, Sunnick E, et al. (2009) Cytotoxicity of metal and semiconductor nanoparticles indicated by cellular micromotility. ACS Nano 3: 213-222.
28. Lin J, Zhang H, Chen Z, et al. (2010) Penetration of lip-

id membranes by gold nanoparticles: insights into cellular uptake, cytotoxicity, and their relationship. ACS Nano 4: 5421-5429.

29. Tan SJ, Jana NR, Gao S, et al. (2010) Surface-ligand-dependent cellular interaction, subcellular localization, and cytotoxicity of polymer-coated quantum dots. Chem Mater 22: 2239-2247.
30. Xia T, Kovochich M, Liong M, et al. (2008) Cationic polystyrene nanosphere toxicity depends on cell-specific endocytic and mitochondrial injury pathways. ACS Nano 2: 85-96.
31. Ryman-Rasmussen JP, Riviere JE, Monteiro-Riviere NA (2006) Penetration of intact skin by quantum dots with diverse physicochemical properties. Toxicol Sci 91: 159-165.
32. Dobrovolskaia MA, McNeil SE (2007) Immunological properties of engineered nanomaterials. Nat Nanotechnol 2: 469-478.
33. Nagy A, Steinbruck A, Gao J, et al. (2012) Comprehensive analysis of the effects of CdSe quantum dot size, surface charge, and functionalization on primary human lung cells. ACS Nano 6: 4748-4762.
34. Arvizo RR, Miranda OR, Thompson MA, et al. (2010) Effect of nanoparticle surface charge at the plasma membrane and beyond. Nano Lett 10: 2543-2548.
35. Sukhanova A, Devy J, Venteo L, et al. (2004) Biocompatible fluorescent nanocrystals for immunolabeling of membrane proteins and cells. Anal Biochem 324: 60-67.
36. Jan E, Byrne SJ, Cuddihy M, et al. (2008) High-Content Screening as a Universal Tool for Fingerprinting of Cytotoxicity of Nanoparticles. ACS Nano 2: 928-938.
37. Wargnier R, Baranov AV, Maslov VG, et al. (2004) Energy transfer in aqueous solutions of oppositely charged CdSe/ZnS core/shell quantum dots and in quantum dot-nanogold assemblies. Nano Lett 4: 451-457.
38. Sukhanova A, Venteo L, Devy J, et al. (2002) Highly stable fluorescent nanocrystals as a novel class of labels for immunohistochemical analysis of paraffin-embedded tissue sections. Lab Invest 82: 1259-1261.
39. Yu WW, Qu L, Guo W, et al. (2003) Experimental determination of the extinction coefficient of CdTe, CdSe, and CdS nanocrystals. Chem Mater 15: 2854-2860.
40. Jasieniak J, Smith L, J van Embden, et al. (2009) Re-examination of the size-dependent absorption properties of CdSe quantum dots. J Phys Chem C 113: 19468-19474.
41. Williams Y, Byrne S, Bashir M, et al. (2008) Comparison of three cell fixation methods for high content analysis assays utilizing quantum dots. J Microsc 232: 91-98.
42. London E, Brown DA (2000) Insolubility of lipids in triton X-100: physical origin and relationship to sphingolipid/cholesterol membrane domains (rafts). Biochim Biophys Acta 1508: 182-195.
43. Diaz B, Sanchez-Espinel C, Arruebo M, et al. (2008) Assessing methods for blood cell cytotoxic responses to inorganic nanoparticles and nanoparticle aggregates. Small 4: 2025-2034.
44. Doose S, Tsay JM, Pinaud F, et al. (2005) Comparison of photophysical and colloidal properties of biocompatible semiconductor nanocrystals using fluorescence correlation spectroscopy. Anal Chem 77: 2235-2242.
45. Sukhanova A, Even-Desrumeaux K, Kisserli A, et al. (2012) Oriented conjugates of single-domain antibodies and quantum dots: toward a new generation of ultrasmall diagnostic nanoprobes. Nanomedicine 8: 516-525.
46. Dawson KA, Salvati A, Lynch I (2009) Nanotoxicology: Nanoparticles reconstruct lipids. Nat Nanotechnol 4: 84-85.
47. Zhang Y, Pan H, Zhang P, et al. (2013) Functionalized quantum dots induce proinflammatory responses in vitro: the role of terminal functional group-associated endocytic pathways. Nanoscale 5: 5919-5929.
48. Barua S, Rege K (2009) Cancer-cell-phenotype-dependent differential intracellular trafficking of unconjugated quantum dots. Small 5: 370-376.
49. Verma A, Uzun O, Hu Y, et al. (2008) Surface-structure-regulated cell-membrane penetration by monolayer-protected nanoparticles. Nat Mater 7: 588-595.
50. Ghitescu L, Fixman A (1984) Surface charge distribution on the endothelial cell of liver sinusoids. J Cell Biol 99: 639-647.
51. Nelson WJ (2003) Epithelial cell polarity from the outside looking in. News Physiol Sci 18: 143-146.

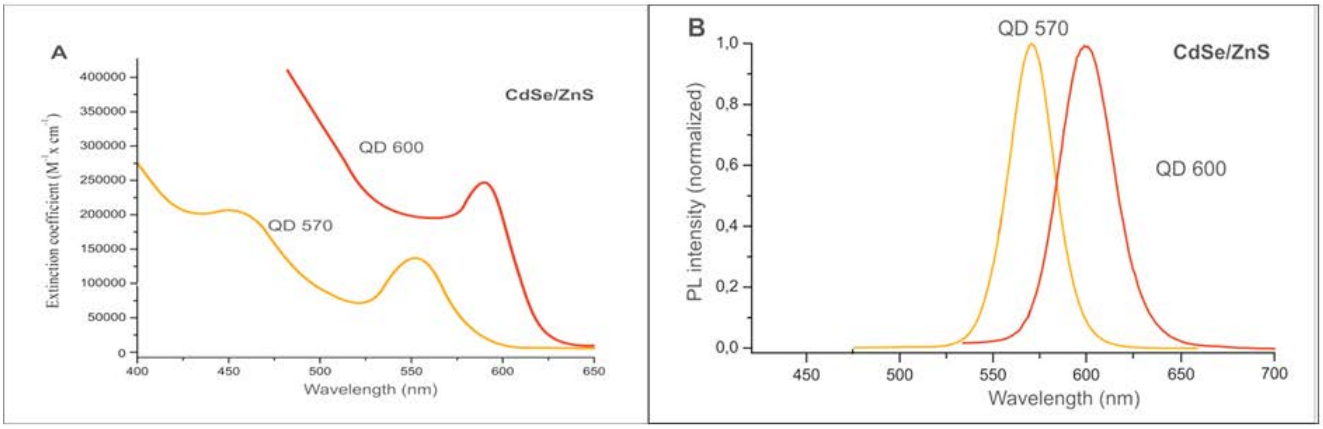

Figure S1: Absorption (S1A) and fluorescence emission (S1B) spectra of CdSe/ZnSQD.
Yellow curves, QD emitting at 570 nm; red curves, QD emitting at 600 nm.

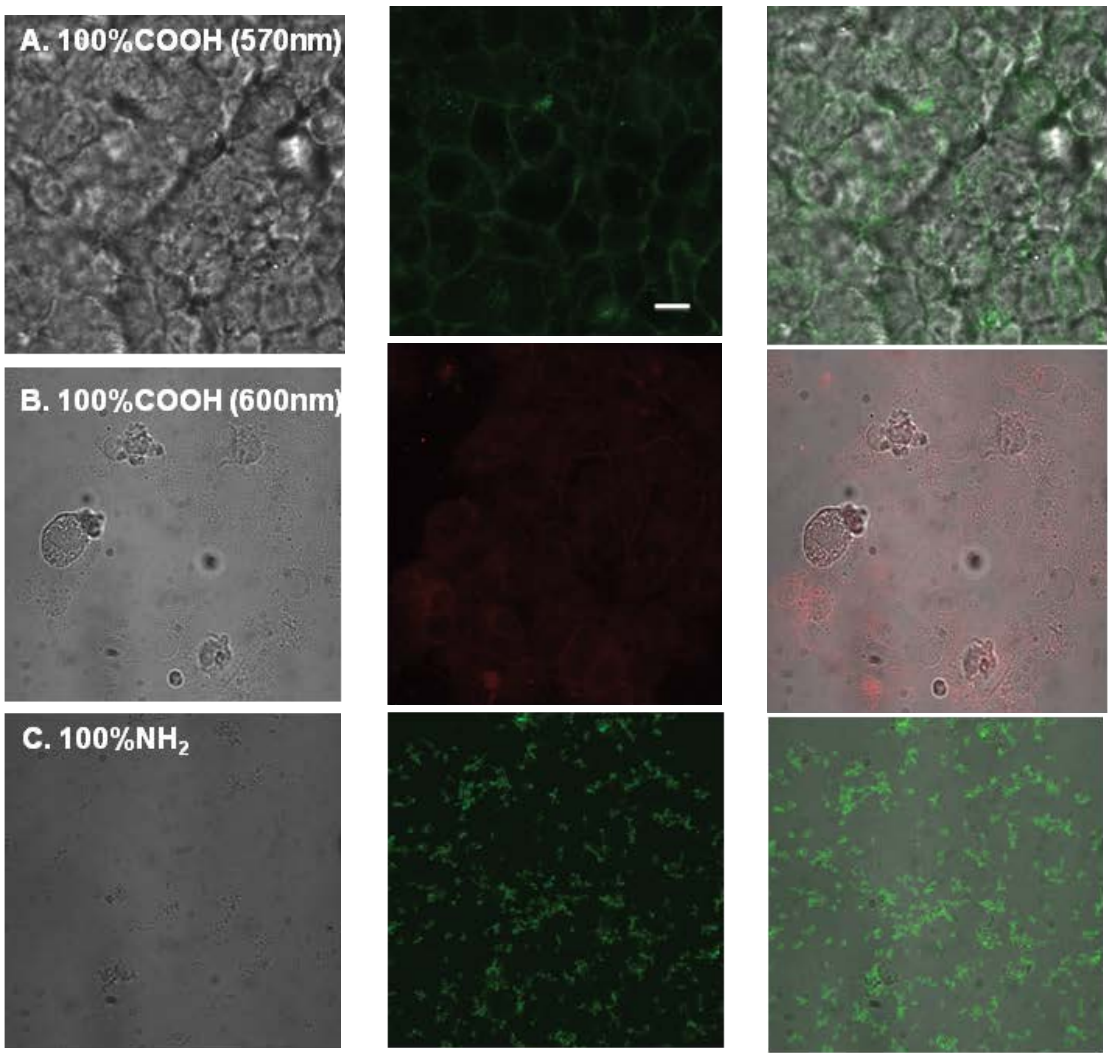

Figure S2: Localization of 100% COOH (570 nm) QDs and 100% COOH (600 nm) QDs and biocompatibility comparison with 100% NH_2QD when exposed to epithelial cells.

(S2A) 100% COOH (570 nm) QD forming a thin line of green fluorescence on the surface of epithelial cells;

(S2B) 100% COOH (600 nm) QD forming a thin line of red fluorescence on the surface of epithelial cells;

(S2C) Aggregates of 100% NH_2QD with no viable cells visible in the field.

Brightfield, fluorescence, and overlay images are shown. These images were captured with an UltraView Live Cell Imager confocal microscopy workstation (PerkinElmer Life Sciences, Warrington, UK) using a ×60 lens. Scale bar is 10 μm.